Proceedings of the Institute of Acoustics

FREQUENCY DIVERSITY VS LARGE BANDWIDTH RECONSTRUCTION: INFORMATION CONTENT FOR NETTED SENSOR ATR USING ISAR IMAGES

M. Vespe Electronic & Electrical Engineering Dept., UCL, London, UK
C. J. Baker Electronic & Electrical Engineering Dept., UCL, London, UK
H. D. Griffiths Electronic & Electrical Engineering Dept., UCL, London, UK

1 INTRODUCTION

The ability to detect and classify radar targets has many crucial applications for both civil and military purposes. As a consequence, a high degree of reliability is required. Most of the approaches to Automatic Target Recognition (ATR) have focused on forming higher and higher spatial resolutions, both in slant-range[1] (1-D) and cross-range[2] (2-D). Research has also been reported investigating the backscattering properties description improvement given by polarimetric information[2,3]. Interest in the utility of angular diversity for improving classification performance has recently come into sight[4-7]. The main motivations are (i) the simplicity for existing systems to acquire such data and (ii) the additional information in multiple perspectives.

High Range Resolution (HRR) is achieved by synthesizing large bandwidths. The information content of the received signal modulated by the target resides not only in the spatial discrimination of the scatterers identifying the target, but also in the scattering behaviour of the radar object when illuminated by a set of different frequencies. In this paper, the information content of radar target signatures is analysed in terms of range resolution (coherent bandwidth reconstruction), Multi-Frequency (M-F) illumination and the corresponding classification performance evaluated using multiple perspectives collected by a network of radars.

In optical images, the illuminating waveform has a wavelength much shorter than the dimension of the elementary structures forming the object. Therefore, optical targets appear as a set of point-like scatterers with the only exception of rare specular reflections. Furthermore, the reduced incidence of end-region scattering behaviours means that the scattering centre radiation pattern will not show pronounced sidelobes. As a result, the optical image is formed by a set of point scatterers which resemble the physical spatial distribution of the surface roughness and discontinuities of the target. The progressive reduction of the illuminating frequency to the radar range (1-40 GHz) implies different scattering behaviours of man-made targets. In the radar optics region, for instance, when the illuminating wavelength λ becomes much smaller than the target size D, radar objects can be seen as a set of independent elementary scatterers coherently contributing to the target radar signature. The simplest canonical shape is the point-like scatterer, characterised by an omnidirectional and uniform radiation when not occluded by other parts of the target. Although ideal, at very high frequencies, the discontinuities on the target surface cause abrupt variation of the induced currents and, therefore, the appearance of the low level scatterers in the radar signature. These scatterers often satisfy the point-like properties. Other scattering mechanisms - such as specular reflection, multiple bounces, edge diffraction, end region effect, and surface waves - characterise a number of canonical shapes. These primitives present peculiar reradiation patterns and an RCS dependent on their physical dimension and structure[8]. For instance, a corner reflector is dominated by multiple reflections and its RCS is in direct proportion with the square of the illuminating frequency. The maximum RCS from a cylinder occur when the incident field is normal to its axis and present a linear proportion with the illuminating frequency. Some scattering shapes show an inverse proportion with frequency. Therefore, if a range of frequencies is spanned to sense the elementary shape, the information gained by the corresponding RCS could be used to discriminate the dominant scattering mechanism. Furthermore, a number of shapes will appear only in a particular set of illuminating frequencies. This concept could be extended to complex targets.

The RCS of complex targets is also highly sensitive to both the incident and scattering directions. This is due to a number of factors responsible for the radar signature variability, and as a consequence of the ATR performance reliability. Measurement noise, caused by thermal noise at the receiver, usually corrupts the radar signatures, as well as Electro-Magnetic Interference (EMI) from other telecommunication systems in the neighbourhood of the receiver. Another source of misclassification is intentional signal interference producing a saturation of false alarm (jamming) at the receiver. A confusing target response can be the consequence of clutter (i.e. the unwanted return of objects surrounding the region of interest) and multi-path (delayed returns due to multiple reflection paths). For HRR profiles, slightly different target orientations, due to rotational or translational motion of the target (assuming no range migration occurs), change the relative phase between scatterers whose returns go into the same range bin and hence cause interference resulting in fluctuations in the range profile. This is known as speckle. The aspect angle is also a factor in determining shadowing phenomena: a number of scatterers may be occluded by other parts of the target (local shadowing) or by other targets (global shadowing) and therefore not be seen by the incident waveform. A portion of the target is therefore unavoidably masked and the signature further corrupted. This may be thought of as a loss of information as it can often result in significant regions of the target not contributing to the measured signature or profile. These factors can be overcome by using multiple uncorrelated signatures from the target, i.e. using different perspectives.

In section 2, the techniques used in order to synthesise High Range Resolution and 2-D imageries from turntable Inverse Synthetic Aperture Radar (ISAR) data are introduced as well as the multi-perspective approximation. The dataset, the population set and the definition of the training and test set are described in section 3. Subsequently, after the definition of the parameters used to evaluate the classifier performance, the results of different approaches to information fusion are presented and discussed in section 4. Finally, section 5 concludes.

2 MULTIPLE FREQUENCIES VS HIGH RESOLUTION

ATR attempts to classify radar targets by exploiting their backscattered information. This is usually expressed either by the Radar Cross Section (RCS), High Range Resolution (HRR) range profiles or 2-D imageries. These parameters are related each other and describe the electromagnetic scattering behaviour. By processing a sequence of 1-D profiles, the 2-D representation of target backscattering can be obtained. The eventual image resolution is influenced by the synthesised bandwidth (range resolution) and aperture (cross-range resolution).

2.1 HRR profiles and Stepped-Frequency Compression

The HRR profile is a one-dimensional imagery of the target comprising multiple resolution cells. To achieve higher range resolution than the common chirp compression, a frequency modulated Stepped-Frequency waveform is employed. This reduces the instantaneous bandwidth requirement while increasing the overall bandwidth. HRR range profiles and 2-D images are both produced by processing a wideband reconstruction of the target reflectivity spectrum in the Frequency-Domain[9,10]. As illustrated in Figure 1, by placing side by side N chirps of bandwidth B having an inter-pulse frequency step equal to $B/2$, it is possible to synthesise a total bandwidth expressed as follows:

$$B_{syn} = (N+1)B/2 \tag{1}$$

A range profile is defined as a time sequence of the vector sum of signals reflected back by different scatterers within a range cell. By matched filtering the Stepped-Frequency waveform a slant range resolution $\Delta r_s = c/(2 \cdot B_{syn})$ is achieved. The received signal is the delayed transmitted pulse, modulated by the target. By adding the compressed individual portions of reflectivity function $\zeta(f)$, the entire spectrum is eventually obtained commensurate with the extended bandwidth.

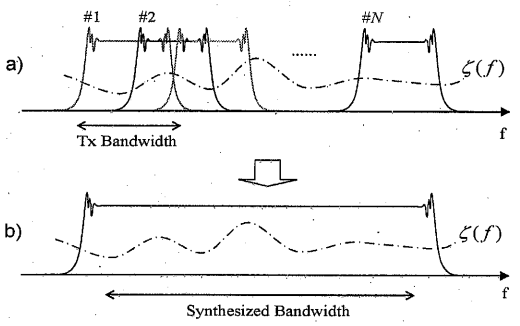

Figure 1: Frequency-Domain reconstruction: sequence of N chirps stepped in frequency (a) and synthesised spectrum (b).

2.2 2-D high resolution imaging

For HRR profiles the resolution achieved in slant-range depends upon the illuminating bandwidth and is normally treated as a one-dimensional image. As regards ISAR systems, the resolution achieved in cross-range depends upon the minimum resolvable frequency between two adjacent scatterers. The Doppler resolution is also related to the available coherent time of integration T which is equal to the time required to collect M profiles. The cross range resolution Δr_c in ISAR systems is a function of the illuminating wavelength λ and the synthesised aperture $\Psi = \omega T$ where ω is the rotational velocity of the target:

$$\Delta r_c = \lambda/(2\omega T) = \lambda/(2\psi) \tag{2}$$

In this paper, the pattern to be classified is deduced from 2-D images obtained by covering apertures $\Psi = 2.83$ degrees. Therefore, the cross-range resolution obtained is approximately 30 cm for all the datasets used. An example of (30 x 30) cm image and the corresponding higher slant range resolution are shown in Figure 2a where the cross-range and range directions can be identified with the vertical and horizontal axes respectively and the radar system is located at the right-hand side of the figure.

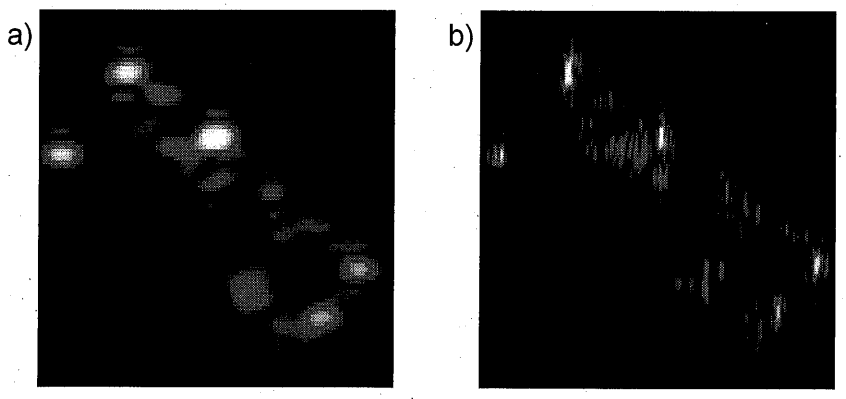

Figure 2: Fixed cross-range resolution (30 cm) ISAR Images from a lorry: (a) single chirp Δr_s = 30cm, (b) Stepped-Frequency Compression Δr_s < 15 cm.

2.3 M-F vs. high resolution

The target reflectivity reconstruction requires the assumption that the target is not moving during the time length of the chirp burst. Therefore, a high PRF is needed between consecutive RF signals. Furthermore, the scattered signature variability due to the speckle may be significant and the

reflectivity reconstruction distorted. As mentioned in the previous section, the advantages in of wideband transmitted signals are the high resolution achievable and the information content of the backscattering at different frequencies. The two aspects will be examined in terms of classification performance.

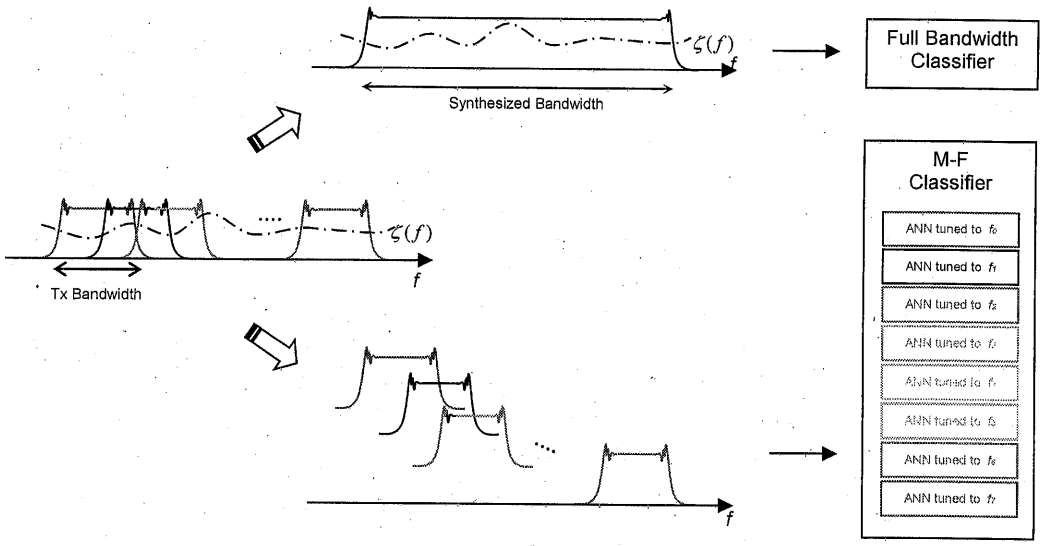

Figure 3: Reflectivity reconstruction and Multi-Frequency classification approaches.

The multiple RF received signatures, as shown in Figure 3, can be considered as separate patterns to be given as input to multiple classifiers tuned to the different centre frequencies. Although the non-exploitation of the higher range resolution and the consequent classification performance deterioration, the M-F approach will allow a more robust and fast processing. Moreover, the resolution obtained by the synthesised wideband is reduced by the clipped side portions of the sub-spectra since the chirps are overlapping (Equation 1), whereas if single chirps are used the sub-spectra are fully utilised.

3 DATASET

ISAR images are formed from a sequence of HRR profiles from turntable measurements. The profiles are generated from an X-band (~10 GHz) radar having an instantaneous bandwidth of 500 MHz, transmitting Stepped-Frequency Compressed pulses. The turntable data is first prepared by removing any stationary clutter to avoid the classifier to exploit this consistent information[11]. Subsequently, 2-D images are formed using the full synthesised bandwidth. Another set of images is formed at lower range resolution for each chirp at different centre frequencies. The cross resolution is maintained constant (~30 cm) for every image by changing the aperture in Equation 2.

3.1 ADAS and MIDAS data: population set

The Airborne Data Acquisition System (ADAS) data-set provided by Thales consists of radar reflectivity frequency samples from three ground vehicles covering 360 degrees of target rotation on a turntable. The reflectivity data from other three targets are obtained by the Mobile Instrumented Data Acquisition System (MIDAS), provided by the former DERA to "La Sapienza" University. As shown in Figure 4, the six targets are organised into four classes (*A*, *B*, *C*, and *D*), plus a confusing class (i.e. not used to train the classifier). The last data file (D_{ind}) corresponds to an independent test target, a different version of the target used to represent class *D* in the training set.

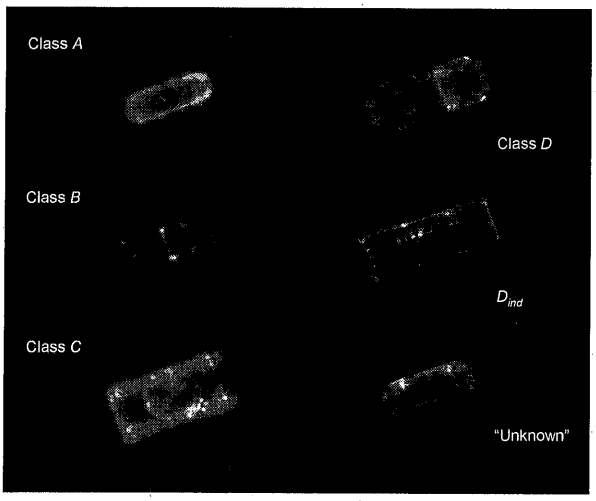

Figure 4: ISAR multi-look images of the ground vehicles dataset.

3.2 Training and test sets

The training set is made up of a sequence of images for each class at specific target's heading. The information content of ground vehicles radar signatures displaced by 180° on the same projection plane shows a minimum from a classification perspective[12]. As a consequence, the training set is formed by 32 images, one every 11° of target rotation, avoiding two representations of the class separated by 180°. The testing set consists of ~350 images separated by ~1°, neglecting the ones used to represent the target in the training set.

4 AUTOMATIC TARGET RECOGNITION

Automatic target Recognition (ATR) can be based either on 1-D range profiles or 2-D images. The former approach is often used for its simplicity in terms of implementation and signal processing. Nevertheless, range profiles give low classification rates if compared to coherently processed imageries which, although the accurate signal processing and the particular movement knowledge requirements of the object, guarantees a more detailed representation of the target backscattering[13]. Each target image is formed synthesising the same aperture Ψ = 2.83 and, therefore, the same cross-range resolution (30 cm). The intensity M x N image is then reshaped into a MN x 1 vector and processed using Principal Component Analysis[14] (PCA), a statistical method that enables the data to be represented in a different vector basis such that it is possible to remove similarities and redundancy within the data. This procedure yield a reduction of the pattern dimension and therefore of the computational burden of the Artificial Neural Network (ANN) classifier during the learning phase.

4.1 ATR Parameters

The classification process typically requires a high probability of correct classification P_{cc}, i.e. the probability of recognising a known target. This is calculated in terms of Correct Classification Rates (CCR) that is the P_{cc} on a finite number of measurements. By defining the probability of declaration P_d as the probability that the classifier makes a decision, P_{cc} becomes the probability of correct classification given that a declaration is made. The probability of missing a target P_{miss} is related to the percentage of not declaring a target used to train the classifier. The declaration properties of a classifier are strictly connected to the unknown threshold specified to determine the rejection of unknown targets.

The output of the non linear mapping of the ANN classifier is an N-unipolar cube $[0,1]^N$ where N is the number of classes forming the population. The decision is made by sensing the greatest component of the output vector which can be therefore considered as a measure of the confidence of the decision. By specifying the uncertainty thresholds, the desired P_d is obtained. The probability of false alarm P_{fa} can be defined as the probability of making a declaration when an unknown target is presented to the classifier. Therefore, when the threshold is set to zero, the classifier is forced to declare (P_d = 1), and the false alarm rate is maximum (P_{fa} = 1). The Receiver Operating Characteristics (ROC) curves represent the relation between the three parameters P_{cc}, P_d, and P_{fa} and will be used to evaluate the ATR classification performance.

4.2 Single-aspect – large bandwidth reconstruction results on 2-D imagery

The classification performance of the classifier using the full synthesised bandwidth obtained by Stepped-Frequency processing the RF chirps is shown in Table 1. The confusion matrix is obtained after fixing a rejection threshold that yields a P_{fa} = 39.6%. The target D_{ind} gives a measure of the generalisation capabilities of the classifier. The probability of declaration is measured as the mean value of (1-ΣP_{miss}) calculated for the classes used to train the classifier and the independent target. P_{fa} is measured on the unknown target only. It is worth noting that the unknown target presents similar shape features to the target of class A, with which it is more likely to be misidentified.

	Output (%)				
↓ Input	*A*	*B*	*C*	*D*	*Unknown*
A	**85.6**	4.4	0.6	0	9.4
B	0.6	**98.3**	0	0	1.1
C	0.3	0	**96.9**	0.9	1.9
D	0.3	0	0.3	**95.3**	4.1
D_{ind}	2.8	13.8	0	**62.7**	20.7
Unknown	22.6	10.6	3.2	3.2	60.4

Table 1: Confusion matrix: P_{fa} = 39.6%, P_d = 92.6%, P_{cc} = 87.8%.

4.3 Single-aspect – Multi-Frequency low resolution results on 2-D imagery

ATR is now approached by using lower resolution ISAR images, first using a single chirp and subsequently applying a data fusion algorithm in order to use multiple frequencies. In Figure 5, the ROC curves of single RFs are compared with different combinations of chirps. The Area Under the Curve (AUC) is a metric for evaluating the classification performance through the ROC curves.

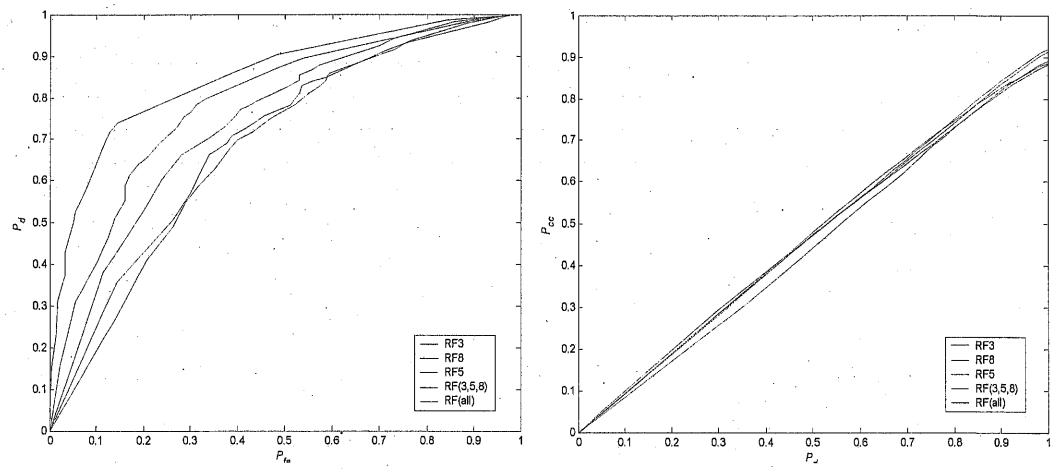

Figure 5: ROC curves for a single chirp at a single frequency and multiple chirps (three and eight).

As anticipated, the classification performance given by particular frequencies appear more robust than others. This is due to the RCS of those features that become more prominent at different illuminating frequencies, making the targets more easily separable in the feature space. Furthermore, a significant classification improvement is achieved by exploiting different RFs.

4.4 Multiple perspectives

The analysis of M-P classification[7,12] shows that the most significant classification improvements are achieved for a relatively small number of nodes in the network and for particularly distributed perspective displacements between the nodes. Considering a relatively small aperture synthesized by a network of radars or by a system flying past the target and collecting multiple views, the two-perspective topology (2-P) $\Delta\varphi_{1,2} = 5°$ and the three-perspective one (3-P) $\Delta\varphi_{1,2} = 5°$; $\Delta\varphi_{1,3} = 10°$ are hereafter analysed. In Figure 6, the resulting ROC curves are represented for the Stepped-Frequency processed images and the corresponding Multi-Frequency chirps. The results using a single view of the target are also reproduced together with the corresponding 2- and 3-P implementations, highlighting the considerable classification performance improvement.

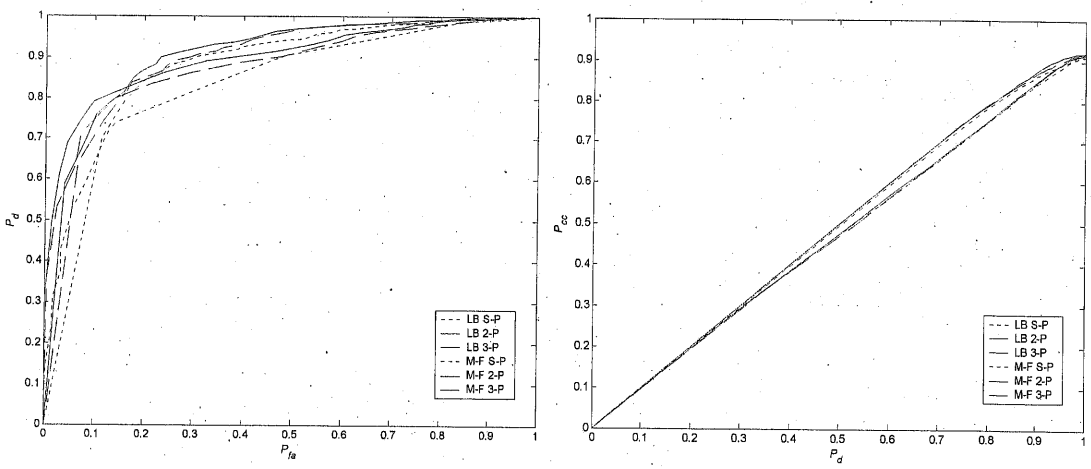

Figure 6: ROC curves for single-perspective (dotted), 2-P (dashed) and 3-P (solid) classifier using large synthesised bandwidth (LB, blue) and eight multiple frequencies (M-F, green).

As can be observed from the relation P_d - P_{cc}, the classifier using the full reconstructed bandwidth exhibits a higher rate of correctly classifying what has been declared. On the other hand, the M-P environment shows its effectiveness on the relation between P_{fa} and P_d : the classification performance improvement is significant for both the reconstructed bandwidth and the M-F approaches when an unknown target is sensed. Moreover, for applications where low P_{fa} are tolerated, the M-F approach guarantees comparable declaration rates with the LB case.

5 CONCLUSION

The classification performance of a Multi-Frequency approach has been compared with the full bandwidth reconstruction methodology and examined using ISAR images from real turntable experiments. The ROC curves of different RF chirps exhibit variable recognition rates, revealing the importance of the backscattered information dependence on the illuminating frequency. The eventual Multi-Perspective implementation of the classifier suggests the significant reliability of the M-F processing, which is (i) more flexible since a particular combination of centre frequencies or a single one based on the highest ATR response can be ad hoc selected; (ii) it is less demanding in terms of processing and target movement knowledge when compared to the full bandwidth reconstruction of the corresponding wideband signal. Nonetheless, the classification results

corroborate the importance of range resolution in terms of classification and the multi-perspective effectiveness independence of the resolution used.

Sonar imagery may require similar considerations since the target dimensions and wavelengths are comparable, although the scattering mechanisms are somewhat different.

6 ACKNOWLEDGEMENTS

The work reported in this paper was funded by the Electro-Magnetic Remote Sensing (EMRS) Defence Technology Centre, established by the UK Ministry of Defence and run by a consortium SELEX Sensors and Airborne Systems, Thales Defence, Roke Manor Research and Filtronic. The authors would like to thank Thales Defence for providing ADAS files to investigate HRR profiles from real targets.

7 REFERENCES

1. Rong Hu and Zhaoda Zhu: 'Researches on radar target classification based on high resolution range profiles', IEEE Aerospace and Electronics Conference, Vol. 2, pp: 951-955, (July 1997).
2. L.M. Novak, S.D. Halversen, G. Owirka, and M. Hiett: 'Effects of polarization and resolution on SAR ATR', IEEE Trans. AES, Vol. 33, No. 1, pp: 102-116, (Jan. 1997).
3. F. Sadjadi: 'Improved target classification using optimum polarimetric SAR signatures', IEEE Trans. AES, Vol. 38, No. 1, pp: 38-49, (Jan. 2002).
4. Ji Shihao, Liao Xuejun and L. Carin: 'Adaptive multiaspect target classification and detection with hidden Markov models', IEEE Sensors Journal, Vol. 5, No. 5, pp: 1035-1042, (Oct. 2005).
5. Xuejun Liao, P. Runkle and L. Carin: 'Identification of ground targets from sequential high-range-resolution radar signatures', IEEE Trans. AES, Vol. 38, No. 4, pp 1230-1242, (Oct. 2002).
6. P.R. Runkle, P.K. Bharadwaj, L. Couchman and L. Carin: 'Hidden Markov models for multiaspect target classification', IEEE Trans. Signal Processing, Vol. 47, No. 7, pp 2035-2040, (July 1999).
7. M. Vespe, C.J. Baker and H.D. Griffiths: 'Radar target classification using multiple perspectives', Journal paper in revision.
8. E.F. Knott, J.F. Shaeffer and M.T. Tuley: *Radar Cross Section*, Artech House, (1985).
9. A.J. Wilkinson, R.T. Lord, and M.R. Inggs: 'Stepped-frequency processing by reconstruction of target reflectivity spectrum', COMSIG '98, pp: 101-104, (Sept. 1998).
10. W. Nel, J. Tait, R. Lord and A. Wilkinson, 'The use of a frequency domain stepped frequency technique to obtain high range resolution on the CSIR X-band SAR system'. IEEE AFRICON. 6th, pp: 327-332, vol. 1, (Oct. 2002).
11. G.A. Showman, M.A. Richards, K.J. Sangston: 'Comparison of two algorithms for correcting zero-Doppler clutter in turntable ISAR imagery', Conference on Signals, Systems & Computers, Vol. 1, pp: 411-415, (1998).
12. M. Vespe, C.J. Baker, H.D. Griffiths: 'Node Location for Netted Radar Target Classification', Proc. 2nd IEEE/IEE Int. Waveform Diversity and Design Conference, Hawaii, (2006).
13. L.M. Novak: 'A Comparison of 1-D and 2-D Algorithms for Radar Target Classification', IEEE International Conference on Systems Engineering, pp 6 -12, (August 1991).
14. S. Theodoridis, and K. Outroumbas: *Pattern Recognition*, Academic Press, (1999).